International Journal of Mechanical Sciences 169 (2020) 105288

Contents lists available at ScienceDirect

International Journal of Mechanical Sciences

journal homepage: www.elsevier.com/locate/ijmecsci

Light-weight shell-lattice metamaterials for mechanical shock absorption

Xueyan Chen [a,b], Qingxiang Ji [a,b], Jianzheng Wei [a], Huifeng Tan [a,*], Jianxin Yu [a], Pengfei Zhang [a], Vincent Laude [b], Muamer Kadic [b]

[a] *National Key Laboratory of Science and Technology on Advanced Composites in Special Environments, Harbin Institute of Technology 92 Xidazhi Street, Harbin, 150001, PR China*

[b] *Institut FEMTO-ST, CNRS, Université Bourgogne Franche-Comté, Besançon 25030, France*

ARTICLE INFO

Keywords:
Metamaterials
Energy absorption
Lattice materials

ABSTRACT

Absorbing mechanical shocks and vibration energy is crucial in industrial, domestic and medical applications. Very often, systems (such as hydraulic cylinders) or structures (such as helmets) are used to achieve energy absorption or protection from impacts or periodic vibrations. In this respect, mechanical metamaterials have received much attention in recent years due to their extraordinary mechanical properties, including outstanding specific stiffness and strength, and energy absorption. Here, we design a stretching-dominated mechanical metamaterial that can absorb very large energies while retaining a low density. In this study, a few examples of metamaterials are considered and we show that a new class of shell lattice (SL) metamaterials has the best mechanical properties for shock absorption they are ultrastiff, ultrastrong, and possess high specific energy absorption at low relative density.

1. Introduction

Absorbing mechanical shocks and vibration energy is crucial in industrial, domestic and medical applications [1–3]. Very often, systems (such as hydraulic cylinder) or structures (such as helmets) are used to achieve energy absorption or protection from impacts or periodic vibrations. In this respect, mechanical metamaterials have received much attention in recent years due to their extraordinary mechanical properties, including outstanding specific stiffness and strength [4–17], and energy absorption [18]. Recently, scientists have shown that metamaterials based on bending-dominated buckling inclusions can absorb more energy than commercially available aluminum foams. This method is very promising, especially when combined with current fabrications techniques such as 3D micro and macro printing. Body-centered cubic (BCC) lattice materials are the best-known bending-dominated materials [19–21]. Such metamaterials, however, lack scalability toward extremely low densities [22] instabilities disappear together with the stiffness. Furthermore, the bending-dominated behavior localizes the plasticity regions toward the hinges.

As cellular materials, mechanical metamaterials are topologically categorized as either bending-dominated or stretching-dominated [23]. The effective mechanical properties of stretching-dominated cellular materials scale linearly with the relative density, unlike bending-dominated materials. Materials deforming in a bending-dominated mode have higher specific energy absorption, but lower stiffness and strength, than those deforming in a stretching-dominated mode.

Octet lattice and truss lattice materials play an important role in stretching-dominated materials [24–28]. Indeed, recent advances in additive manufacturing technology make it possible to fabricate them at the microscale, or even at the nanoscale [29–31]. He et al. showed that surface effects have little influence on the stiffness and strength scaling of nano-lattices [32]. However, stress concentrations often occur at the connections between micro hollow struts in lattice structures.

As an alternative to octet lattice materials, shellular materials, which are composed of a single, periodic, continuous, smooth-curved shell [33], overcome the nodal weaknesses of truss structures and can have an ultralow density. Their compressive response is superior to those of octet lattices at equal relative densities [34–36]. Maskery et al. fabricated gyroid shellular material whose specific energy absorption was nearly three times that of BCC lattice material [37]. Bonatti et al. designed shellular materials with nearly two times the strength and the energy absorption of conventional octet lattices at 20% relative density [38].

Here, we design a stretching-dominated mechanical metamaterial that can absorb very large energies while at the same time retaining a low density. In this study, a few examples of lattice materials are considered and we show that a new class of BCC shellular metamaterials has the best mechanical properties for shock absorption: they are

* Corresponding author.
E-mail address: tanhf@hit.edu.cn (H. Tan).

https://doi.org/10.1016/j.ijmecsci.2019.105288
Received 22 April 2019; Received in revised form 28 August 2019; Accepted 27 October 2019
Available online 6 November 2019

ultrastiff, ultrastrong, and possess high specific energy absorption at a low relative density. The mechanical properties are calculated numerically and verified experimentally under uniaxial compression. Compared to octet lattice metamaterials, our metamaterial has a relative elastic modulus 2.4 times larger and a relative compressive strength about 5.4 times larger, for a relative density of 10%.

2. Design and fabrication of metamaterials

One of the crucial limiting aspect in 3D buckling/absorbing metamaterials is the ratio between the volume of material that is really used (for deformation of absorption) compared to the total volume of the host material. In other words, one needs to optimize all hinges and bending parts such that they deform homogeneously. Obviously, the simplest candidate would be the homogeneous material itself. However, one also needs to decrease the volume and thus to create inner holes. Holes thus become the real playground for optimization. We show in Fig. 1 the stiffness and the potential energy absorption that one can aim at using standard bending-dominated metamaterials versus stretching-dominated materials. The stretching-dominated mechanism appears clearly as a much better candidate for energy absorption.

Figs. 2 (a) and (c) display the geometry of the bending-dominated truss-lattice (TL) metamaterial and its corresponding unit cell model which consists of eight struts. Here, the cross-section of each strut is assumed to be circular with a constant diameter d and a length l. As presented by Ushijima et al., the relative density of the TL metamaterial is the ratio of the actual volume occupied by the lattice structure to the volume of the overall structure [19], or

$$\bar{\rho} = \frac{3\sqrt{3}\pi}{4}\left(\frac{d}{l}\right)^2. \tag{1}$$

However, the above analytical relationship is only valid for TL metamaterials with very low relative density. At high relative density, the influence of material overlap at the nodes cannot be neglected. Subtracting the overlap volume at the nodes, a more precise expression for the relative density is [20]

$$\bar{\rho} = \frac{3\sqrt{3}\pi}{4}\left(\frac{d}{l}\right)^2 - \frac{9\sqrt{2}}{2}\left(\frac{d}{l}\right)^3. \tag{2}$$

Fig. 2 (b) and (d) show a configuration of stretching-dominated shell-lattice (SL) metamaterials and its corresponding unit cell model. The SL unit cell is composed of a spherical shell, which has circular openings on the eight lateral corners, and of four cylindrical shells. The adjacent parts are connected by a smooth variable cross-section cylindrical shell. The unit cell model can be geometrically described by four main parameters, that are the radius of the spherical shell R, the radius of the cylindrical shell r, the length of the cylindrical shell l_0, and the wall thickness t. With a given inclination angle of 30°, the radius of the variable cross-section cylindrical shell is given by

$$r_0 = 2R - r \tag{3}$$

and the total length of the shell strut is expressed as

$$l = l_0 + 2\sqrt{3}(R - r). \tag{4}$$

Hence, the analytical expression for the relative density of SL metamaterial is

$$\bar{\rho} = \frac{V}{\left(\frac{2}{\sqrt{3}}l\right)^3} \tag{5}$$

where V is the unit cell volume of the SL metamaterial and is given by

$$V = V_c + V_s, \tag{6}$$

with the volume of the cylinder shell struts

$$V_c = 8\pi(2r - t)l_0 t \tag{7}$$

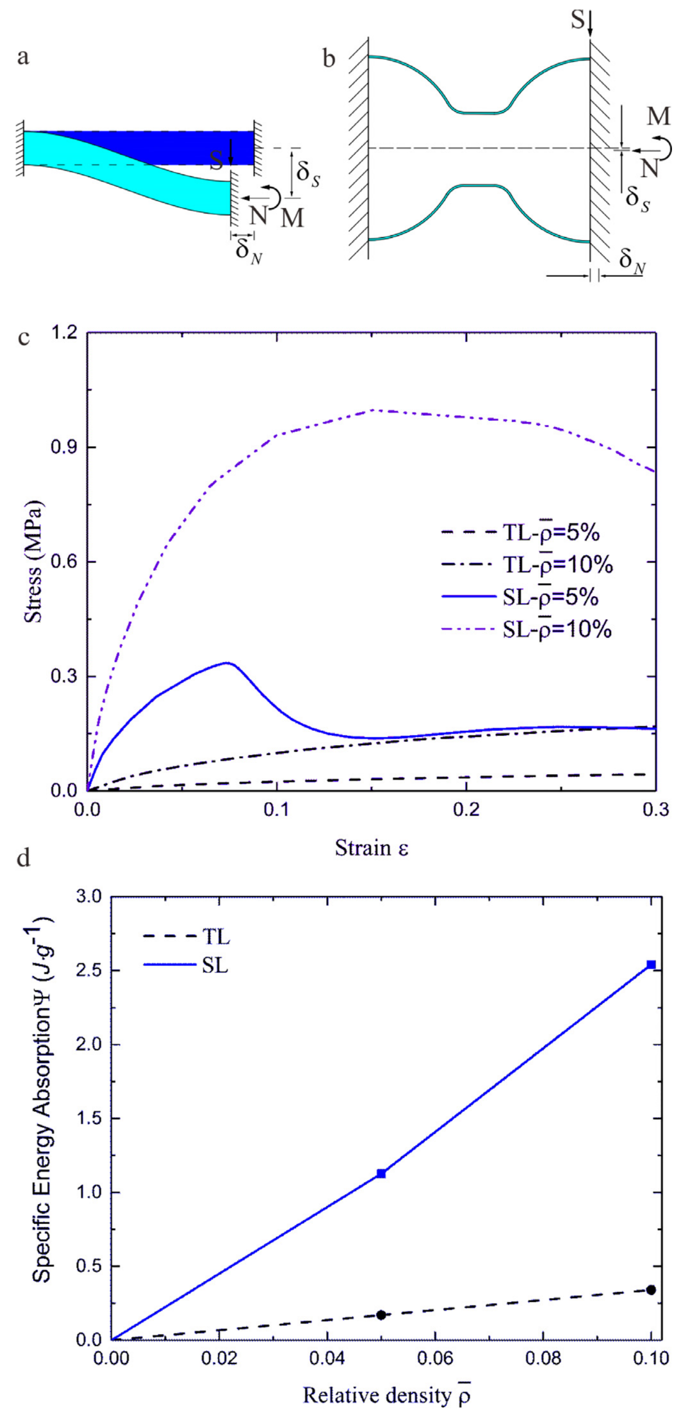

Fig. 1. Simplified doubly clamped beam model of (a) bending-dominated truss-lattice (TL) metamaterial and of (b) variable cross-section shell model of stretching-dominated shell-lattice (SL) metamaterial. Deformations under axial compressing force, bending moment and shearing load are shown. Under the same loading conditions, the shell model appears to have less axial and deflection displacements than the beam model. (c) Compressive stress-strain curves obtained from finite simulations. SL has higher elastic modulus and strength than TL. (d) The specific energy absorption (SEA) of SL is almost 4 times larger at low relative density.

and the volume of the spherical shell nodes

$$V_s = 8\pi t\left[\frac{4}{3}\pi(R-r)^2 + \left(4\sqrt{3} - \frac{2\pi}{3}\right)(R-r)(2r-t) - 3R(R-t) - t^2\right]. \tag{8}$$

We designed stretching-dominated shell-lattice (SL) metamaterials and compared them to standard bending-dominated truss-lattice (TL)

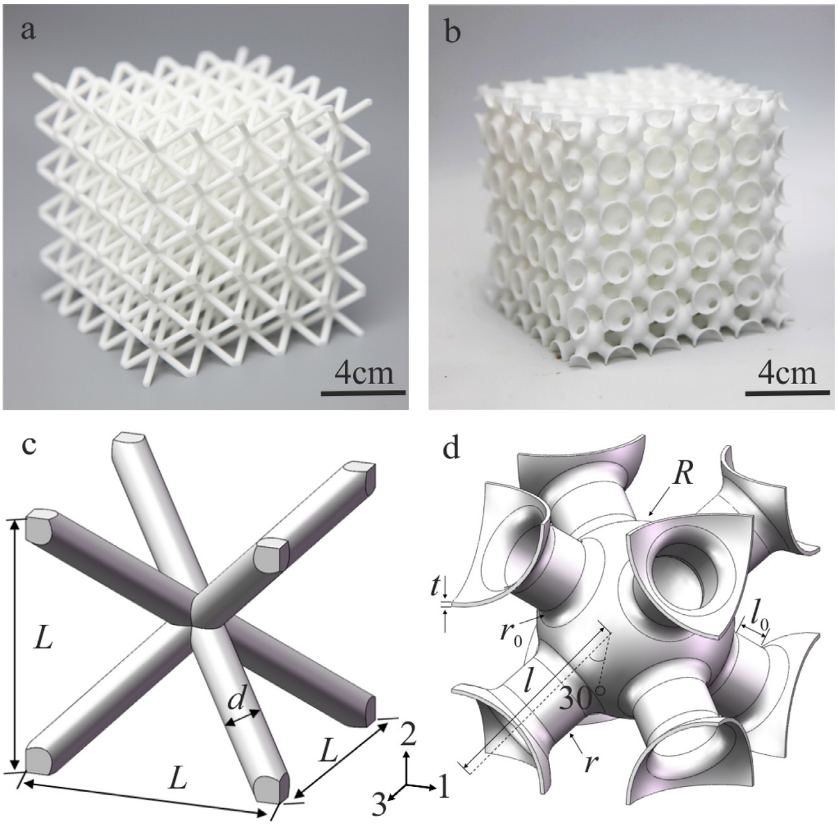

Fig. 2. Representative photographs of (a) bending-dominated TL and (b) stretching-dominated SL samples are shown. The unit-cells of (c) TL and (d) SL metamaterials have a base-centered cubic (BCC) symmetry. Important geometrical parameters are shown.

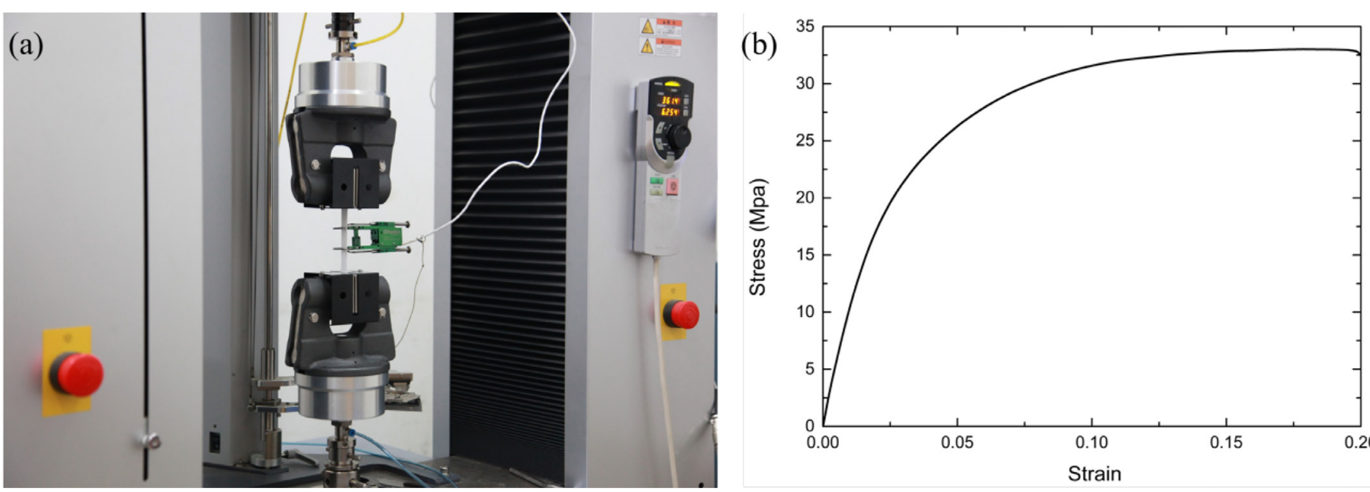

Fig. 3. (a) Measurement setup for the uniaxial tensile test on the printed dog-bone specimens. (b) Stress-strain curve of the tensile specimen.

metamaterials. Samples were fabricated by selective laser sintering (SLS) using a 3D printer (EOS model P110) with the base material PA 2200 (EOS Nylon 12), using a laser power of 30 W and a scanning speed of 5 m/s. The operational temperature was 190 °C and the layer thickness was 0.06 mm. Representative samples and their unit-cells are displayed in Fig. 2. As a note, all structures presented here are anisotropic due to cubic symmetry. We only consider in experiments the (1,0,0) direction, which is one of three principal directions and the strongest of them, as representative for the investigation of the compressive response. Each specimen comprises $5 \times 5 \times 5$ unit cells and features a strut length $l = 17.32$ mm. Three configurations and relative densities $\bar{\rho} = 0.05$ or 0.10 were investigated. Configuration TL has strut diameter $d = 1.01$ mm or 1.45 mm (Fig. 2a and c). Two different SL configurations were selected in order to investigate the effect of parameters R/r and $l_0/(l - l_0)$ on mechanical properties. Configuration SL1 is composed of small ball shells and long cylindrical shell struts ($R = 6.94$ mm, $r = 2.78$ mm, $l_0/(l - l_0) = 0.2$). The wall thickness t is either 0.29 mm or 0.59 mm. Configuration SL2 is composed of large ball shells and short cylindrical shell struts ($R = 8.04$ mm, $r = 3.5$ mm, $l_0/(l - l_0) = 0.1$). The wall thickness t is either 0.23 mm or 0.56 mm. For each configuration, two samples were manufactured for uniaxial compression experiments. The maximum dimensional error between as-designed and measured samples was 0.8%. As a note, the smallest relative density of about 5% was imposed by fabrication constraints.

3. Characterization

To obtain the mechanical properties of parent material PA2200, five dog-bone specimens were manufactured according to the ASTM 638 standard with the same laser processing as used to build lattice and

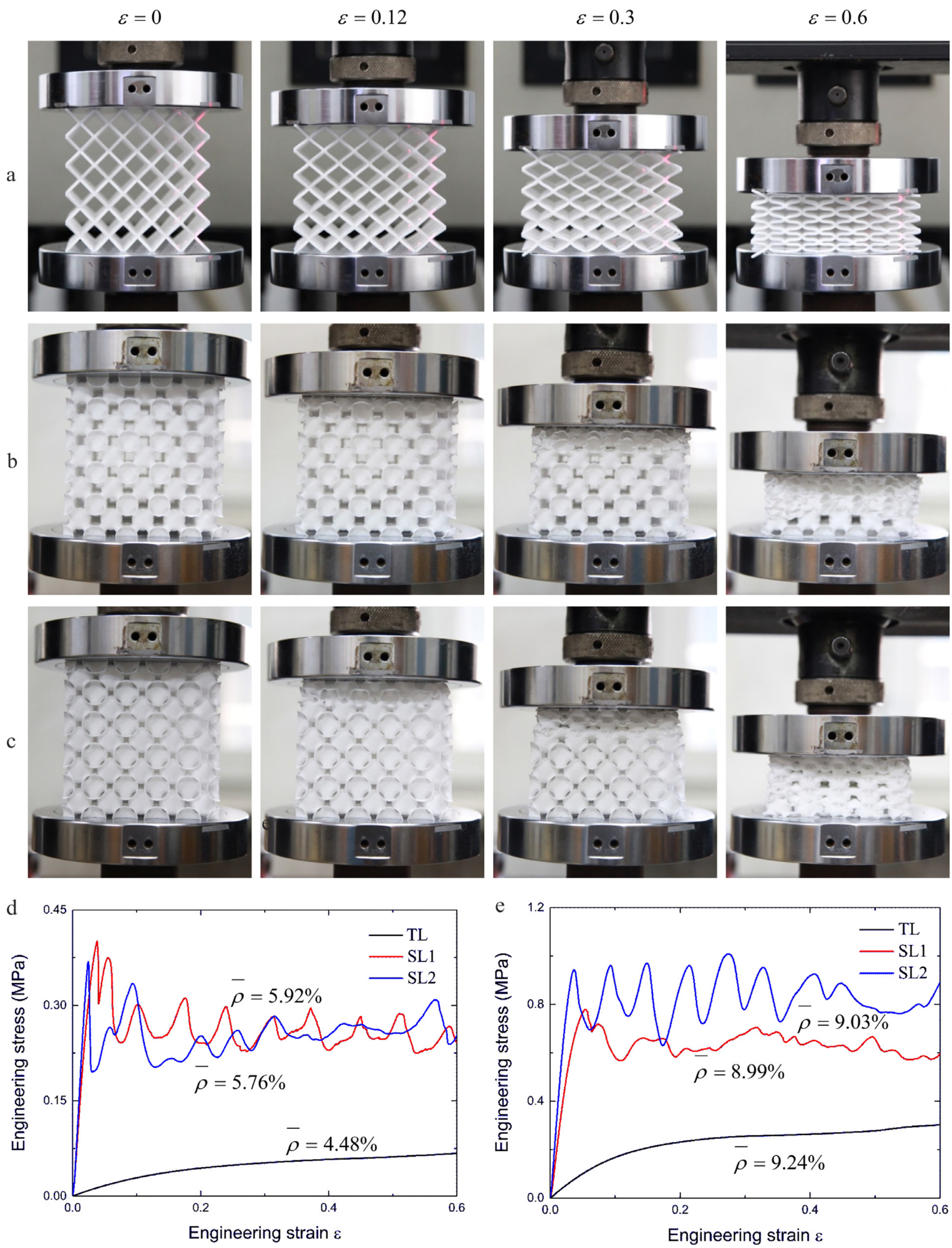

Fig. 4. Compressive deformations of (a) TL, (b) SL1 and (c) SL2 samples are shown as a function of strain. For strains of 0.12, top and bottom surfaces of the TL sample are not entirely in contact with the compression platens. The error from this defect in the applied load is likely to be small, and certainly far less than the effect of geometry which can be neglected. The particular photographs shown are for a relative density of 5%. (corresponding images for a relative density of 10% are shown in Figure S1). Engineering stress-strain curves are shown for a relative density of 5% in panel (d) and 10% in panel (e).

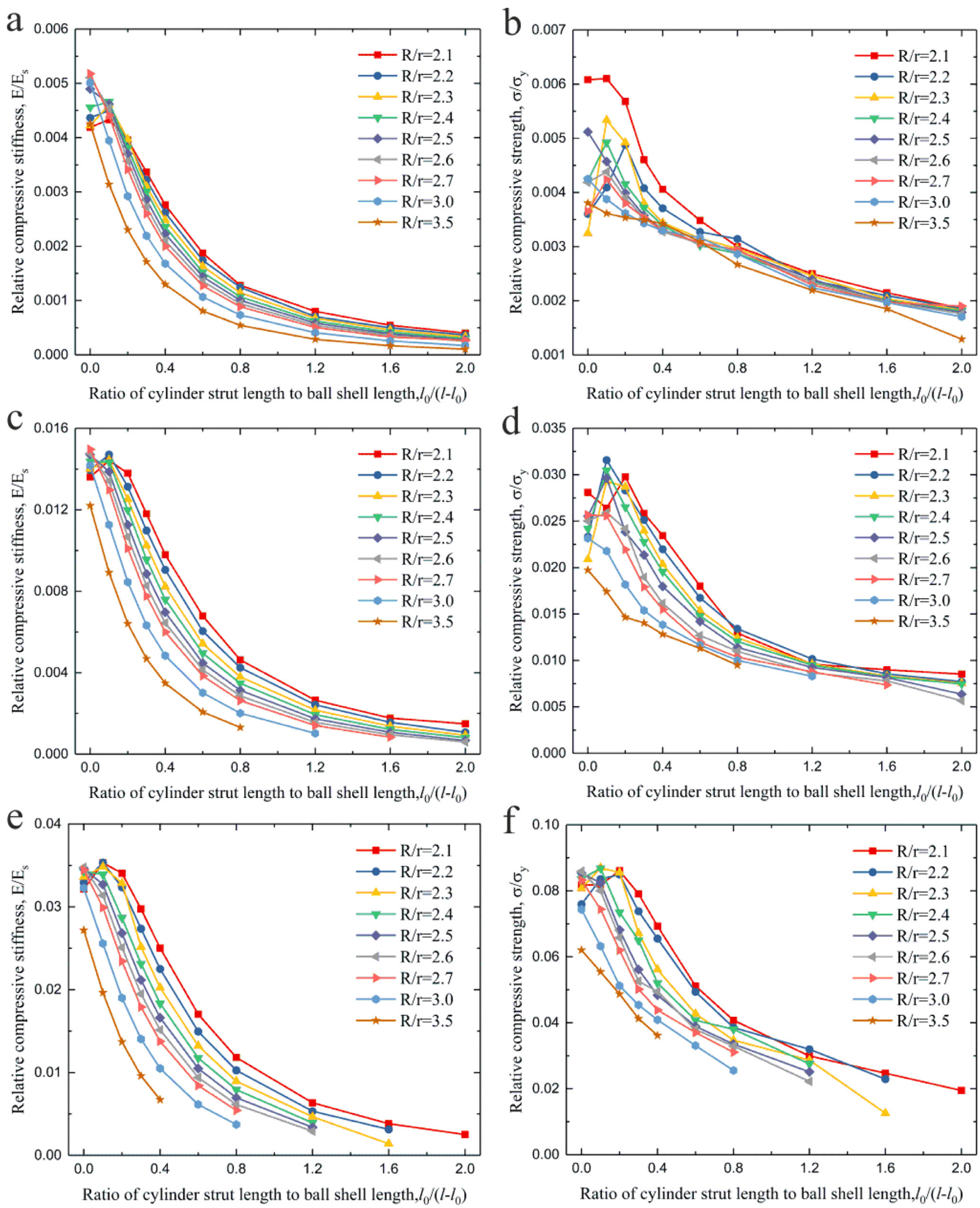

Fig. 5. Optimization of SL metamaterial: the compressive stiffness and strength of SL metamaterial with relative densities of 0.02, 0.05 and 0.10 are plotted as a function of geometrical parameters R/r and $l_0/(l - l_0)$.

shellular structures for uniaxial tensile test. The uniaxial tensile test on the printed dog-bone specimens were performed on a 5 kN SHMADZU testing machine at a nominal strain rate of 10^{-3} s^{-1}. The axial tensile deformations of the tested specimens were measured by a mechanical gripping type extensometer. Fig. 3(b) shows the stress-strain curve of the tensile specimen. The average elastic modulus is about 1.17 GPa and the 0.2% offset yield stress is nearly 14.09 MPa. The ultimate strength is about 33 MPa and the corresponding strain is 20%.

Once fabricated, samples were experimentally tested under uniaxial loading. Quasi-static compression tests were conducted on an Instron machine with 50 kN load cell at a nominal strain rate of 10^{-3} s^{-1}. Samples were positioned between two polished steel platens with suitable preload forces applied to ensure no slip. During the test, samples were placed in the center of the loading device to avoid the influence of eccentric forces. Tests were continued until the onset of densification. Engineering stresses were calculated by dividing measured loads by the specimen cross sections. Engineering strains were obtained by dividing the displacement of the moving platen by the specimen height.

Fig. 4 (a)–(d) shows compressive deformations of the samples at a relative density of 5%. The TL sample exhibits a monotonically increasing engineering compressive response. After an initial linear phase, the stress-strain curve turns into a weakly increasing elastic-plastic phase. After an initial elastic phase followed by an infinitesimal nonlinear increasing behavior, the response of SL1 reaches a first peak stress of about 0.4 MPa followed by buckling oscillations. The main differences between SL1 and SL2 are that the first hump of SL2 has lower amplitude and its elastic modulus is larger. For both SL samples, a weakly damped oscillation stress-strain response can be observed. During the compression test, the struts of the TL sample are mainly subjected to bending moments, whereas the deformation of the TL samples are uniform. It is observed that the SL samples are collapsing from upper to lower boundaries in a layer by layer fashion.

Fig. 4 (e) shows compressive deformations of the samples at a relative density of 10%. The compressive response of TL and SL1 samples show trends similar to those at 5% relative density. Their collapsing modes are also unchanged. Interestingly, SL2 at 10% relative density has the highest modulus and strength among all configurations. SL2 collapses from upper and lower boundaries to middle plane in a layer by layer fashion. The deformation mode is also more stable compared with other configurations and there is no obvious attenuation in amplitude oscillations.

4. Simulation

A series of unit-cell models with different relative densities were built using the commercial finite element software ABAQUS with first-order solid elements (type C3D8R). The constituent material (PA 2200) was assumed to be isotropic and is modeled as a perfectly elasto-plastic material. The stress-strain curve is obtained from a tensile test. For PA 2200, Poisson's ratio is usually set to be 0.4. For all models, the edge length of unit cells is fixed to 2 mm. The corresponding strut diameter for TL and wall thickness for SL change with relative density. For the SL unit cell, there are four solid elements along the wall thickness direction at low relative density. Five solid elements through thickness were used in high relative density models. To improve the calculation accuracy, periodic boundary conditions are applied. The compressive strength due to yield and buckling is extracted from the simulations. Buckling strengths were obtained by eigenvalue buckling analysis, following Valdevit et al. [39]. The yield strength can be defined as the first peak in the stress-strain curve calculated by elastic-plastic analysis. For the TL metamaterial, $\epsilon = 7\%$ is chosen as the collapsing strain and the corresponding strength is taken as the yield strength.

5. Results and discussion

The parameters chosen for SL metamaterials were obtained from numerical analysis and are optimal for the chosen relative densities. Fig. 5 shows the variation of the relative compressive stiffness and of the strength of SL metamaterials as a function of geometrical parameters R/r and $l_0/(l-l_0)$.

When R/r is smaller than 2.5, a tiny increase followed by a continuous decrease in elastic modulus is found. When R/r is larger than 2.5, the compressive modulus is a monotonic decreasing function of $l_0/(l-l_0)$. When $l_0/(l-l_0)$ is larger than 0.2, the compressive modulus decreases with R/r. Similar trends are found in Fig. 5(c) and (e). The only difference is that the transition value of R/r decreases as the relative density increases.

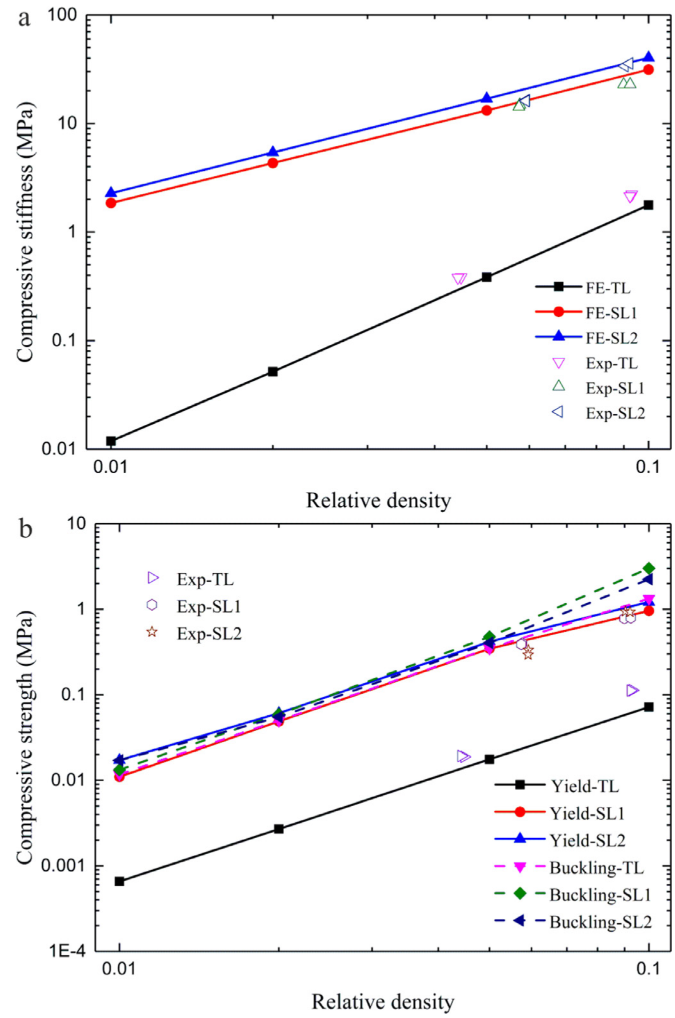

Fig. 6. Evolution of compressive stiffness (a) and strength (b) as obtained from experiments and finite element simulations as a function of relative density for TL, SL1 and SL2 metamaterials.

Similarly, the maximum compressive strengths are always found for $l_0/(l-l_0)$ smaller than 0.3. However, compared with the stiffness curves, the variations of compressive strength are more disordered at small R/r. That may contribute to the occurrence of local buckling at low relative density, which decreases the compressive strength significantly. The main conclusion of this analysis is that in order to achieve the best compressive performance the interval of geometrical parameters is $R/r = 2.1$ to 2.5 and $l_0/(l-l_0) = 0.1$ to 0.3.

We compared experimental results to numerical simulations and found them to be in good agreement (see Fig. 6). With an increase in relative density, the compressive stiffness and strength of all three configurations increase. SL2 has the largest stiffness. The elastic modulus of TL is always much less than that of SL. When the relative density is smaller than 5%, SL1 possesses the highest compressive strength. At high relative densities, the compressive strength of SL2 is in contrast significantly higher than that of SL1.

Fig. 7 displays the failure modes of TL, SL1 and SL2 metamaterials with relative densities ranging from 0.01 to 0.1 under uniaxial compressive loading. SL metamaterials always fail by plastic collapse of the struts before the onset of elastic buckling. The strength of TL is always much less than that of SL1 and SL2 materials. The stress concentration is located at the connections of adjacent struts where plastic hinges occur.

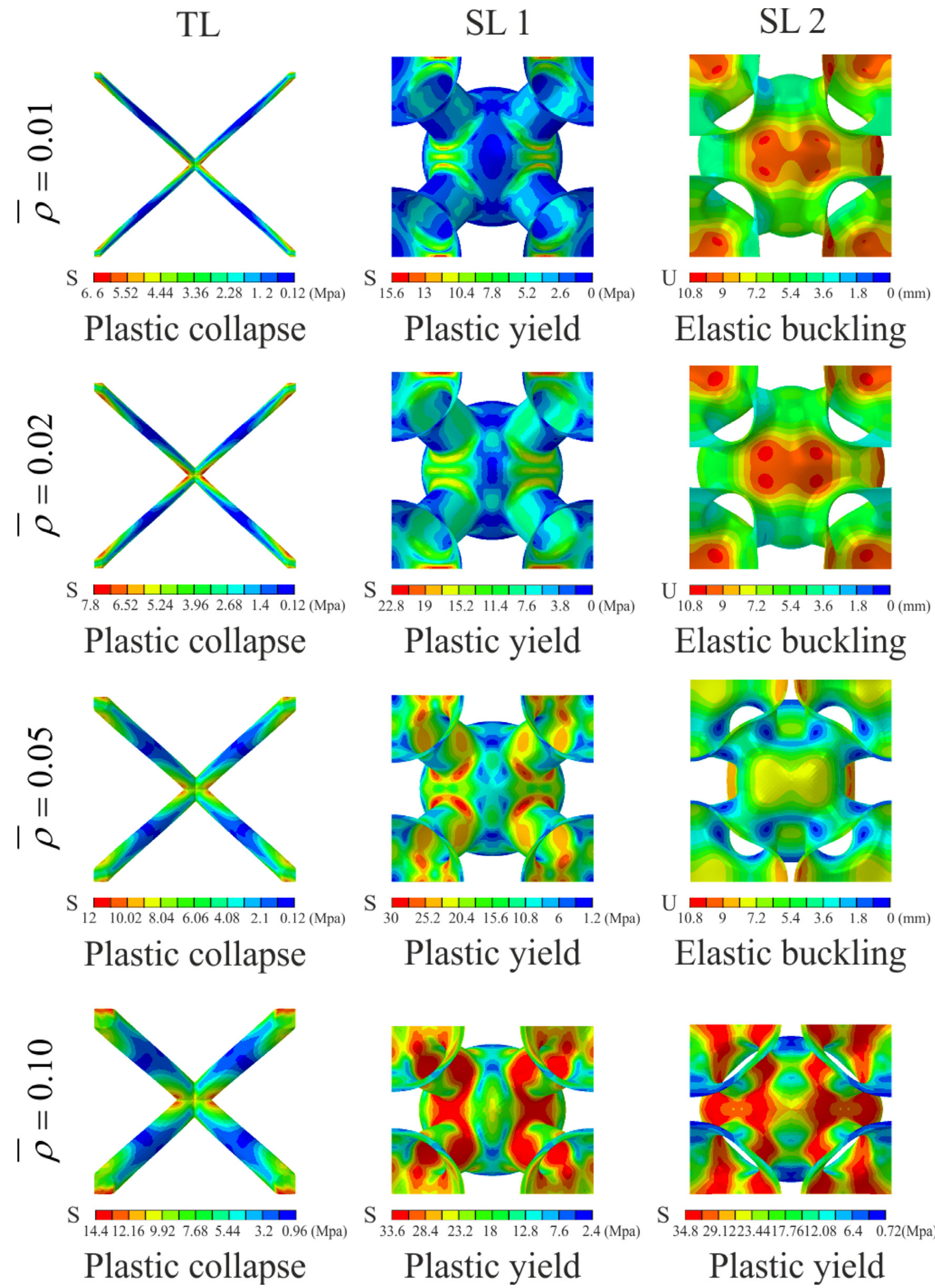

Fig. 7. Failure mode of TL, SL1 and SL2 metamaterials with relative densities ranging from 0.01 to 0.1 under uniaxial compressive loading.

The appearance of plastic hinges can guarantee the stability of mechanical performance, but at the expense of reducing the structure capability. The failure of SL1 structures is dominated by plastic yield, not by elastic buckling. At low relative densities, the SL1 structure possesses the highest compressive strength and the stress concentration is located near variable cross-section cylindrical shells. With a relative density increase, the range of stress concentration extends to shell struts. Different from TL and SL1 metamaterials, SL2 metamaterials fail by elastic buckling or plastic yield, as determined by the relative density. When the relative density is smaller than 5%, the buckling strength is close to the yield strength and stress concentration is always located at the middle areas of the ball shells. Spherical shells are too thin to resist local buckling

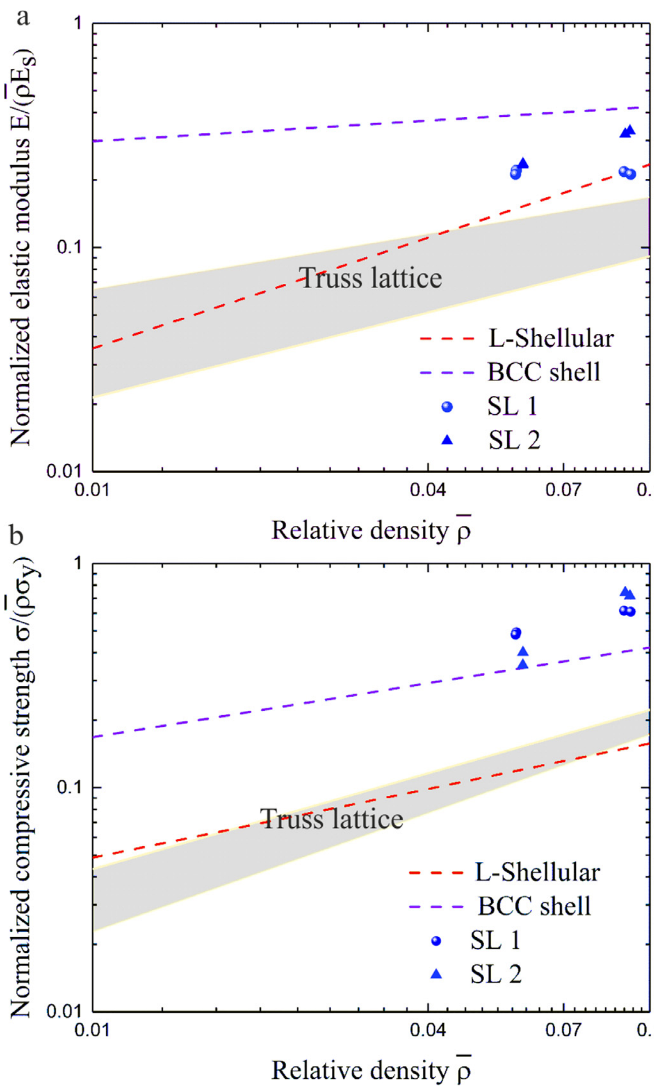

Fig. 8. Comparison of normalized (a) elastic modulus and (b) strength between our SL samples and other stretching-dominated lattice and shellular materials, including octet truss-lattice [41], L-shellular [36], and BCC shellular [40] metamaterials.

and the failure of the SL2 metamaterial is dominated by local buckling of spherical shells. Note that in our simulations the elastic buckling strength and the yield strength of SL1 are very close to that of SL2 at low relative density. The strength of SL2 should be larger than that of SL1. However, SL2 structures are more sensitive to flaws, imperfections and boundary effects due to their structural characteristics, that is, the ratio of wall thickness and ball shell radius is too small. Hence, as compared to the SL1 material, the load bearing capacity of SL2 is good but not improved. However, at high relative density the compressive strength of SL2 is significantly higher than that of SL1, which is validated by the previous experiments. Stress concentration is located at most areas of spherical shells and cylinder strut shells. Of course, flaws, imperfections and boundary effects are also the most important factors, but they have less effect on compressive strength as the wall thickness increases. Moreover, the advantage of a large ratio of spherical radius to cylinder strut length is more obvious.

We also compared the effective stiffness and strength with other stretching-dominated lattice materials and other shellular materials [36,39,40], as reported in Fig. 8. For a fair comparison between different constituent materials, we use the normalized elastic modulus $E/(\bar{\rho}E_S)$ and the normalized compressive stress $\sigma/(\bar{\rho}\sigma_Y)$. SL metamaterials have higher relative compressive stiffness and strength (see Fig. 8). For relative density of about 10%, SL2 metamaterial has a relative strength about 5.4 times and a relative elastic modulus about 2.4 times larger than those of octet lattice material [41], which makes it a noteworthy alternative to support structures.

Finally, the specific energy absorption (SEA), a crucial characteristics of any shock absorber, is defined as the work performed under uniaxial compression up to a strain of −0.6 per gram of mass by

$$\mathrm{SEA} = \frac{V\int_0^{0.6}\sigma d\epsilon}{M}. \tag{9}$$

The SEA is obtained experimentally from compressive stress-strain curves (see Fig. 3). At low relative density, the SEA of the SL1 metamaterial is almost 4 times larger than the SEA of the BCC lattice material and is slightly larger than the SEA of the SL2 metamaterial. When the relative density is about 9%, the SL2 metamaterial has a SEA nearly 3.56 times as large as the SEA of the BCC metamaterial and nearly 1.26 times as large as the SEA of the SL1 metamaterial. In absolute numbers for the low density of 5% we get $SEA_{\mathrm{TL}} = 0.61$ J/g, $SEA_{\mathrm{SL1}} = 2.71$ J/g and $SEA_{\mathrm{SL2}} = 2.61$ J/g and for the high density of 10% we get $SEA_{\mathrm{TL}} = 0.47$ J/g, $SEA_{\mathrm{SL1}} = 4.15$ J/g and $SEA_{\mathrm{SL2}} = 5.23$ J/g. Lately, a paper by Bonatti et al. [40] reported results similar to ours, but for metallic structures. In comparison, we achieve a lower normalized elastic modulus (normalization is to the constituent material in order to enable a fair comparison of the designed metamaterials) but a larger normalized compressive strength with much cheaper fabrication technique and constituent materials.

6. Conclusion

As a conclusion, we have designed a stretching-dominated mechanical metamaterial that are ultrastiff, ultrastrong, and that exhibit high specific energy absorption properties at low relative density. These stretching-dominated mechanical metamaterials can absorb large energies while at the same time retaining a low density. They are promising candidates for applications to shock absorption and as a model for closed-cell crystalline foams.

Acknowledgments

This work was supported by the Foundation for Innovative Research Groups of the National Natural Science Foundation of China(grant number 11421091); and Fundamental Research Funds for the Central Universities (grant number HIT.MKSTISP.2016 09). M.K. and V.L. acknowledge support by the EIPHI Graduate School (contract ANR-17-EURE-0002) and the French Investissements dAvenir program, project ISITEBFC (contract ANR-15-IDEX-03).

Supplementary material

Supplementary material associated with this article can be found, in the online version, at 10.1016/j.ijmecsci.2019.105288.

References

[1] . Phononic crystals. Khelif A, Adibi A, editors. Amsterdam: Springer; 2016.
[2] Babaee S, Viard N, Wang P, Fang NX, Bertoldi K. Acoustic switches: harnessing deformation to switch on and off the propagation of sound. Nat Rev Mater 2016;28(8). 1630–1630
[3] Craster RV, Guenneau S. Acoustic metamaterials: negative refraction, imaging, lensing and cloaking. Springer Science & Business Media; 2012.
[4] Gibson LJ, Ashby MF. Cellular solids: structure and properties. Cambridge University Press; 1999.
[5] Grima JN, Jackson R, Alderson A, Evans KE. Do zeolites have negative poisson's ratios? Adv Mater 2000;12(24):1912–18.
[6] Milton GW. The theory of composites. Cambridge University Press; 2002.
[7] Grima JN, Alderson A, Evans KE. Negative poissons ratios from rotating rectangles. Comput Methods Sci Technol 2004;10(2):137–45.
[8] Bertoldi K, Reis PM, Willshaw S, Mullin T. Negative poisson's ratio behavior induced by an elastic instability. Advanced Material 2010;22(3):361–6.

[9] Overvelde JTB, Shan S, Bertoldi K. Compaction through buckling in 2d periodic, soft and porous structures: effect of pore shape. Advanced Material 2012;24(17):2337–42.
[10] Grima JN, Caruana-Gauci R, Dudek MR, Wojciechowski KW, Gatt R. Smart metamaterials with tunable auxetic and other properties. Smart Mater Struct 2013;22(8):084016.
[11] Babaee S, Shim J, Weaver JC, Chen ER, Patel N, Bertoldi K. 3D soft metamaterials with negative Poisson's ratio. Adv Mater 2013;25(36):5044–9.
[12] Bertoldi K, Vitelli V, Christensen J, van Hecke M. Flexible mechanical metamaterials. Nat Rev Mater 2017;2(11):17066.
[13] Coulais C, Sounas D, Alù A. Static non-reciprocity in mechanical metamaterials. Nature 2017;542(7642):461.
[14] Coulais C, Sabbadini A, Vink F, van Hecke M. Multi-step self-guided pathways for shape-changing metamaterials. Nature 2018;561(7724):512.
[15] Vyatskikh A, Delalande S, Kudo A, Zhang X, Portela CM, Greer JR. Additive manufacturing of 3d nano-architected metals. Nat Commun 2018;9(1):593.
[16] Qu J, Kadic M, Wegener M. Three-dimensional poroelastic metamaterials with extremely negative or positive effective static volume compressibility. Extreme Mech Lett 2018;22:165–71.
[17] Kadic M, Milton GW, van Hecke M, Wegener M. 3D metamaterials. Nature Rev Phys 2019:1.
[18] Schaedler TA, Ro CJ, Sorensen AE, Eckel Z, Yang SS, Carter WB, Jacobsen AJ. Designing metallic microlattices for energy absorber applications. Adv Eng Mater 2014;16(3):276–83.
[19] Ushijima K, Cantwell WJ, Mines R, Tsopanos S, Smith M. An investigation into the compressive properties of stainless steel micro-lattice structures. J Sandwich Struct Mater 2011;13(3):303–29.
[20] Gümrük R, Mines R. Compressive behaviour of stainless steel micro-lattice structures. Int J Mech Sci 2013;68:125–39.
[21] Tancogne-Dejean T, Mohr D. Stiffness and specific energy absorption of additively–manufactured metallic BCC metamaterials composed of tapered beams. Int J Mech Sci 2018;141:101–16.
[22] Schaedler TA, Jacobsen AJ, Torrents A, Sorensen AE, Lian J, Greer JR, Valdevit L, Carter WB. Ultralight metallic microlattices. Science 2011;334(6058):962–5.
[23] Deshpande VS, Ashby MF, Fleck NA. Foam topology: bending versus stretching dominated architectures. Acta Mater 2001;49(6):1035–40.
[24] Deshpande VS, Fleck NA, Ashby MF. Effective properties of the octet-truss lattice material. J Mech Phys Solids 2001;49(8):1747–69.
[25] Mohr D. Mechanism-based multi-surface plasticity model for ideal truss lattice materials. Int J Solids Struct 2005;42(11–12):3235–60.
[26] Elsayed MSA, Pasini D. Multiscale structural design of columns made of regular octet-truss lattice material. Int J Solids Struct 2010;47(14–15):1764–74.
[27] Tancogne-Dejean T, Spierings AB, Mohr D. Additively-manufactured metallic micro-lattice materials for high specific energy absorption under static and dynamic loading. Acta Mater 2016;116:14–28.
[28] Chen XY, Tan HF. An effective length model for octet lattice. Int J Mech Sci 2018;140:279–87.
[29] Zheng X, Lee H, Weisgraber TH, Shusteff M, DeOtte J, Duoss EB, Kuntz JD, Biener MM, Ge Q, Jackson JA, et al. Ultralight, ultrastiff mechanical metamaterials. Science 2014;344(6190):1373–7.
[30] Meza LR, Das S, Greer JR. Strong, lightweight, and recoverable three-dimensional ceramic nanolattices. Science 2014;345(6202):1322–6.
[31] Gu XW, Greer JR. Ultra-strong architected cu meso-lattices. Extreme Mech Lett 2015;2:7–14.
[32] He Z, Wang F, Zhu Y, Wu H, Park HS. Mechanical properties of copper octet-truss nanolattices. J Mech Phys Solids 2017;101:133–49.
[33] Schoen AH. Infinite periodic minimal surfaces without self-intersections. Washington, USA: NASA-TN-D-5541, C-98; 1970.
[34] Han SC, Lee JW, Kang K. A new type of low density material: shellular. Adv Mater 2015;27(37):5506–11.
[35] Lee MG, Lee JW, Han SC, Kang K. Mechanical analyses of shellular, an ultralow–density material. Acta Mater 2016;103:595–607.
[36] Nguyen BD, Cho JS, Kang K. Optimal design of shellular, a micro-architectured material with ultralow density. Mater Des 2016;95:490–500.
[37] Maskery I, Aboulkhair NT, Aremu AO, Tuck CJ, Ashcroft IA. Compressive failure modes and energy absorption in additively manufactured double gyroid lattices. Addit Manuf 2017;16:24–9.
[38] Bonatti C, Mohr D. Large deformation response of additively-manufactured FCC metamaterials: from octet truss lattices towards continuous shell mesostructures. Int J Plast 2017;92:122–47.
[39] Valdevit L, Godfrey SW, Schaedler TA, Jacobsen AJ, Carter WB. Compressive strength of hollow microlattices: experimental characterization, modeling, and optimal design. J Mater Res 2013;28(17):2461–73.
[40] Bonatti C, Mohr D. Smooth-shell metamaterials of cubic symmetry: anisotropic elasticity, yield strength and specific energy absorption. Acta Mater 2019;164:301–21.
[41] Meza LR, Phlipot GP, Portela CM, Maggi A, Montemayor LC, Comella A, Kochmann DM, Greer JR. Reexamining the mechanical property space of three-dimensional lattice architectures. Acta Mater 2017;140:424–32.